

Extended Reflection Waveform Inversion via Differential Semblance Optimization

Yujin Liu*, William W. Symes[†] and Zhenchun Li*, *China University of Petroleum (Huadong), [†]Rice University

SUMMARY

Reflection-based waveform inversion introduces migration and demigration process to retrieve low-wavenumber component from reflection data, but both difference- and correlation-based methods suffer from the cycle-skipping problem when the time shifts change rapidly. In this abstract, we introduce model extension and differential semblance optimization into reflection-based waveform inversion. With another degree of freedom in the model space, we can eliminate the time difference between synthetic and observed data so the cycle skipping problem is avoided. Differential semblance operator is used to detect the incoherence of the extended model. The hybrid objective function, consisting of data misfitting and differential semblance term, shows better convexity than only data misfitting term. We propose a two-stage scheme to minimize the hybrid objective function, that is, the inner loop to update extended the reflectivity and the outer loop to update the background velocity. In order to accelerate the convergent rate of the two-stage scheme, we propose two different approximations of diagonal Hessian and use them as preconditioners in the inner and outer loop respectively. With numerical tests, we show the importance of linearized inversion in the inner loop and also demonstrate that our proposed method can successfully recover both high- and low-wavenumber components of the subsurface model. Even though we specify the model extension in the subsurface offset domain and ignore non-linear effects, other extensions and non-linear inversion are also possible under the same framework.

INTRODUCTION

With the fast development of computational technology in recent years, Waveform Inversion (WI) (Tarantola, 1984) retrieves its popularity in exploration seismology. It can provide detailed information about the subsurface model by minimizing the difference between synthetic and observed data. However, it can not estimate the low-wavenumber background model if there is no sufficient low frequencies in seismic data (Virieux and Operto, 2009). Meanwhile, the ability of WI to recover high-wavenumber model depends on an accurate background model. If the initial background model is far from the true one, WI suffers from cycle skipings and is prone to local minima problem.

Various methods are proposed to handle cycle skipping problem. Multiscale approaches (Bunks et al., 1995) recursively add higher-wavenumber details to models started from low-frequency data, but it's useful only if sufficient low frequencies are available. Laplace domain WI (Shin and Cha, 2008) uses damped wavefields to recover low-wavenumber model, but long offset information is still necessary for deep-layer inversion. Compared with WI, traveltimes inversion (Luo and Schuster, 1991) can better resolves the low-wavenumber com-

ponent because the traveltimes shift is more sensitive and more linearly related to low-wavenumber model. Traveltimes inversion has successfully applied in transmission case, where only first arrivals are used, it's still difficult to recover low-wavenumber components in deep depth if there is no sufficient long offset information in seismic data.

In order to recover low-wavenumber components in deep layers, we should make use of reflection wave. However, compared with transmission wave, reflection traveltimes is more difficult to extract, especially in very complex geological settings. Manually picking arrivals is prohibitively time-consuming and is prone to manual errors. More automatic approaches, such as cross-correlation (Luo and Schuster, 1991; Van Leeuwen and Mulder, 2010) and dynamic image warping (Ma and Hale, 2013) methods, are proposed to estimate the time shifts, but they still might suffer from the cycle skipping problem when the time shifts change very rapidly.

One the other hand, waveform-based method is also possible to recover low-wavenumber components in deep depth even though there is no low frequency. Xu et al. (2012) and Zhou et al. (2012) proposed Reflection-based Waveform Inversion (RWI) by migration and demigration process, but it's also prone to local minimum as conventional WI method due to the limitation of the objective function. Another indirect way is switching the objective function into image domain and back-projecting the incoherence information of the reflectivity image into background velocity update, which is well-known as Wave-Equation Migration Velocity Analysis (WEMVA) (Biondi and Sava, 1999; Shen and Symes, 2008).

In this abstract, we introduce model extension and differential semblance optimization into RWI and propose to minimize a two-term objective function to recover both low- and high-wavenumber components of subsurface model. We show that our proposed method, namely extended reflection waveform inversion (ERWI), relates WEMVA and RWI theoretically and immune to local minimum problem. Numerical tests demonstrate the effectiveness of our proposed method.

THEORY

Objective function of ERWI

WI estimates subsurface model \mathbf{m} by minimize the difference between modeling data $\mathbf{F}[\mathbf{m}]$ and observed data \mathbf{d} , that is,

$$\min_{\mathbf{m}} J_{WI}[\mathbf{m}] = \frac{1}{2} \|\mathbf{F}[\mathbf{m}] - \mathbf{d}\|^2 \quad (1)$$

in which the symbol $\|\cdot\|^2$ stands for ℓ_2 norm. While extended waveform inversion introduce model extension $\bar{\mathbf{m}}$ and minimize the difference between extended modeling data $\bar{\mathbf{F}}[\bar{\mathbf{m}}]$ and observed data \mathbf{d} , that is,

$$\min_{\bar{\mathbf{m}}} J_{EWI}[\bar{\mathbf{m}}] = \frac{1}{2} \|\bar{\mathbf{F}}[\bar{\mathbf{m}}] - \mathbf{d}\|^2 \quad (2)$$

ERWI

After adding another degree of freedom, EWI can eliminate larger time difference between synthetic and observed data, but the model is non-physical. In order to make the solution of EWI physical, we solve the following inverse problem,

$$\min_{\tilde{\mathbf{m}}} J_{EWI}[\tilde{\mathbf{m}}] = \frac{1}{2} \|\tilde{\mathbf{F}}[\tilde{\mathbf{m}}] - \mathbf{d}\|^2 + \frac{\sigma}{2} \|\mathbf{A}\tilde{\mathbf{m}}\|^2 \quad (3)$$

where \mathbf{A} is annihilator to minimize the non-physical energy of the extended model (Symes, 2008).

Split the extended model $\tilde{\mathbf{m}}$ into low-wavenumber component (background model) \mathbf{b} and high-wavenumber component (reflectivity model) \mathbf{r} and only extend the high-wavenumber model, that is,

$$\tilde{\mathbf{m}} \simeq \mathbf{b} + \tilde{\mathbf{r}} \quad (4)$$

When the background model is smooth and is close to the true model, the extended forward map operator can be linearized by Born approximation, that is,

$$\tilde{\mathbf{F}}[\tilde{\mathbf{m}}] \simeq \tilde{\mathbf{F}}[\mathbf{b}] + \tilde{\mathbf{L}}\tilde{\mathbf{r}} \quad (5)$$

where $\tilde{\mathbf{L}}$ is Linearized Extended Born Modeling (LEBM) operator, which is the first derivative of $\tilde{\mathbf{F}}$ with respect to $\tilde{\mathbf{m}}$. Then, the previous inverse problem switches to the linearized version,

$$\min_{\tilde{\mathbf{r}}, \mathbf{b}} J_{LEWI}[\tilde{\mathbf{r}}, \mathbf{b}] = \frac{1}{2} \|\tilde{\mathbf{L}}\tilde{\mathbf{r}} - \mathbf{d}_0\|^2 + \frac{\sigma}{2} \|\mathbf{A}\tilde{\mathbf{r}}\|^2 \quad (6)$$

where $\mathbf{d}_0 = \mathbf{d} - \tilde{\mathbf{F}}[\mathbf{b}]$, σ is the penalty parameter. When $\sigma \rightarrow 0$, Equation 6 limits to the problem of Migration Velocity Analysis (MVA); when $\sigma \rightarrow \infty$, Equation 6 limits to the problem of Least-Squares Migration (LSM) with respect to reflectivity model and Reflection-based Waveform Inversion (RWI) with respect to background model.

Gradient computation

The gradient of the objective function 6 with respect to the high-wavenumber component is,

$$\nabla_{\tilde{\mathbf{r}}} J_{LEWI}[\tilde{\mathbf{r}}, \mathbf{b}] = \tilde{\mathbf{L}}^T (\tilde{\mathbf{L}}\tilde{\mathbf{r}} - \mathbf{d}_0) + \mathbf{A}^T \mathbf{A}\tilde{\mathbf{r}} \quad (7)$$

where $\tilde{\mathbf{L}}^T$ is the adjoint of LEBM operator, which is also called Extended Reverse-Time Migration (ERTM) operator. On the other hand, the gradient of the objective function 6 with respect to the low-wavenumber component is,

$$\nabla_{\mathbf{b}} J_{LEWI}[\tilde{\mathbf{r}}, \mathbf{b}] = \mathbf{B}[\tilde{\mathbf{r}}, \tilde{\mathbf{L}}\tilde{\mathbf{r}}_k - \mathbf{d}_0] \quad (8)$$

where \mathbf{B} is bilinear operator, which means that it's linearly related with both input vectors, that is inverted extended reflectivity $\tilde{\mathbf{r}}_k$ and data misfit $\tilde{\mathbf{L}}\tilde{\mathbf{r}}_k - \mathbf{d}_0$ after k iterations. The detail of the derivation can be found in the abstract (Liu et al., 2013a).

Approximation of diagonal Hessian

Hessian of the two-term objective function with respect to extended reflectivity has been well discussed in previous abstract (Liu et al., 2013b). In this section, we focus on Hessian of the two-term objective function with respect to background velocity. If we fix the extended reflectivity in the input vectors of bilinear operator, the background velocity perturbation is linearly related with data perturbation, that is,

$$\Delta \mathbf{d} = \mathbf{T} \Delta \mathbf{b} \quad (9)$$

where \mathbf{T} is also called tomographic operator (Almomin and Biondi, 2013). The explicit solution of $\Delta \mathbf{b}$ for the linear inverse problem is,

$$\Delta \mathbf{b} = (\mathbf{T}^T \mathbf{T})^{-1} \mathbf{T}^T \Delta \mathbf{d} \quad (10)$$

where $\mathbf{T}^T \mathbf{T}$ is Hessian for wave-equation tomography. The diagonal elements can be approximated using the following formula,

$$\mathbf{H}_d = \mathbf{T}^T \mathbf{T} \mathbf{1} \quad (11)$$

where $\mathbf{1}$ is a constant velocity perturbation field that has unit value everywhere. The approximation is similar to the method proposed by (Shen and Symes, 2013) but in the data domain. Then we apply the diagonal of Hessian to scale the gradient, that is,

$$\Delta \mathbf{b} = \mathbf{g}_b / \mathbf{H}_d = \mathbf{T}^T \Delta \mathbf{d} / \mathbf{H}_d \quad (12)$$

Shaping regularization (Fomel, 2007) is used to avoid zero division.

Two-stage inversion scheme

We develop two-stage inversion scheme to solve the inverse problem 6. The first stage is to solve a linear inverse problem to get the inverted extended reflectivity. The second stage is to solve a non-linear inverse problem to get the updated background model. Approximation of diagonal Hessians are used to precondition both stages to accelerate the convergent rate. The detail of the two-stage scheme is shown in algorithm 1.

Algorithm 1 Two-stage scheme of ERWI

- 1: given initial background model \mathbf{b}_0
- 2: input seismic reflection data \mathbf{d}_0
- 3: **for** $i = 0 \cdots niter$ **do**
- 4: solve the sub-LS problem for $\tilde{\mathbf{r}}_k^i$ and $\tilde{\mathbf{L}}\tilde{\mathbf{r}}_k^i - \mathbf{d}_0$
- 5: compute the gradient $\mathbf{g}_b^i = \nabla_{\mathbf{b}} J_{LEWI}[\tilde{\mathbf{r}}_k^i, \mathbf{b}]$
- 6: scale the gradient $\Delta \mathbf{b}^i = \mathbf{g}_b^i / \mathbf{H}_d$
- 7: update the background model $\mathbf{b}^{i+1} = \mathbf{b}^i - \alpha \Delta \mathbf{b}^i$
- 8: **end for**
- 9: output inverted background model $\mathbf{b}^{niter+1}$
- 10: output inverted extended reflectivity $\tilde{\mathbf{r}}_k^{niter+1}$

Acoustic constant density medium case

In this section, we provide explicit formula of operator $\tilde{\mathbf{L}}$, $\tilde{\mathbf{L}}^T$ and \mathbf{B} in acoustic constant density medium. The model $m(\mathbf{x})$ is defined as squared slowness. We extend the model along subsurface offset domain and split the extended model $\tilde{m}(\mathbf{x}, \mathbf{h})$ into background model $b(\mathbf{x})$ and extended reflectivity $r(\mathbf{x}, \mathbf{h})$. The formula of LEBM operator is

$$\begin{aligned} d(\mathbf{x}_r, \mathbf{x}_s, \omega) = \\ -\omega^2 f(\omega) \int d\mathbf{x} d\mathbf{h} G(\mathbf{x}_r, \mathbf{x} + \mathbf{h}, \omega) r(\mathbf{x}, \mathbf{h}) G(\mathbf{x} - \mathbf{h}, \mathbf{x}_s, \omega) \end{aligned} \quad (13)$$

where \mathbf{x} is the space vector, \mathbf{h} is the subsurface offset vector, \mathbf{x}_s is the source position, \mathbf{x}_r is the receiver position, ω is the frequency, $f(\omega)$ is the spectrum of source function. $G(\mathbf{x}, \mathbf{x}_s, \omega)$ is the Green function satisfying the following wave equation,

$$(\nabla^2 + \omega^2 b(\mathbf{x})) G(\mathbf{x}, \mathbf{x}_s, \omega) = \delta(\mathbf{x} - \mathbf{x}_s) \quad (14)$$

ERWI

The adjoint of LEBM operator is,

$$r(\mathbf{x}, \mathbf{h}) = - \int d\mathbf{x}_s d\mathbf{x}_r d\omega \omega^2 f^*(\omega) G^*(\mathbf{x}_s, \mathbf{x} - \mathbf{h}, \omega) G^*(\mathbf{x} + \mathbf{h}, \mathbf{x}_r, \omega) d(\mathbf{x}_r, \mathbf{x}_s, \omega) \quad (15)$$

which is ERTM formula and also the space shift imaging condition (Rickett and Sava, 2002; Biondi and Symes, 2004).

Similarly, we add a small perturbation $\Delta b(\mathbf{x})$ to the initial background model $b_0(\mathbf{x})$, that is,

$$b(\mathbf{x}) = b_0(\mathbf{x}) + \Delta b(\mathbf{x}) \quad (16)$$

and apply linear approximation, we can get the formula of bi-linear operator,

$$\begin{aligned} \Delta b(\mathbf{y}) = & \int d\mathbf{x}_s d\mathbf{x}_r d\mathbf{x} d\mathbf{h} d\omega \left\{ G_0(\mathbf{y}, \mathbf{x}_s, \omega) \omega^4 f(\omega) \right\}^* \\ & \left\{ G_0^*(\mathbf{y}, \mathbf{x} - \mathbf{h}, \omega) r(\mathbf{x}, \mathbf{h}) G_0^*(\mathbf{x} + \mathbf{h}, \mathbf{x}_r, \omega) \Delta d(\mathbf{x}_r, \mathbf{x}_s, \omega) \right\} + \\ & \int d\mathbf{x}_s d\mathbf{x}_r d\mathbf{x} d\mathbf{h} d\omega \left\{ G_0(\mathbf{y}, \mathbf{x} + \mathbf{h}, \omega) r(\mathbf{x}, \mathbf{h}) G_0(\mathbf{x} - \mathbf{h}, \mathbf{x}_s, \omega) \omega^4 f(\omega) \right\}^* \\ & \left\{ G_0^*(\mathbf{y}, \mathbf{x}_r, \omega) \Delta d(\mathbf{x}_r, \mathbf{x}_s, \omega) \right\}. \end{aligned} \quad (17)$$

The physical meaning of the operator can be explained as: the first term is the cross-correction between background source wavefield and perturbed receiver wavefield; the second term is the cross-correction between perturbed source wavefield and background receiver wavefield. As both terms cross-correct wavefields propagating in the same direction, low-wavenumber components information can be recovered. If we restrict the offset to be zero, the formula 17 is equivalent to the gradient formula of background velocity in difference-based reflection waveform inversion.

NUMERICAL TEST

Behaviors of the hybrid objective function

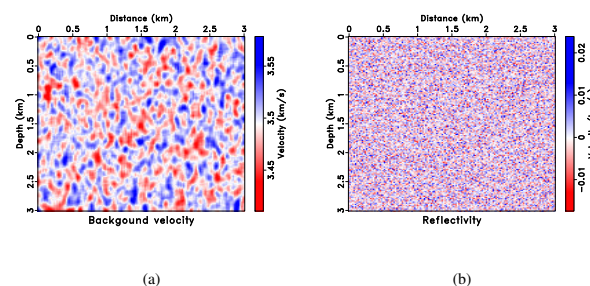


Figure 1: (a) Background velocity; (b) Reflectivity.

Firstly, we use random background velocity and reflectivity to investigate the behaviors of our proposed objective function with respect to background model. The true background model and reflectivity are shown in figure 1(a) and figure 1(b)

respectively. A Ricker wavelet with a fundamental frequency of 15 Hz and temporal sampling of 0.75 ms is used as a source function to model the data. There are 151 fixed receivers with a spacing of 20 m and 31 sources with a spacing of 100 m. The maximum offset used is 1.5 km in both sides.

We calculate the objective function with scanning velocity $v = \mu v^*$, where v^* is the correct velocity, μ is a scaler varied from 0.85 to 1.1. The first term, second term and total one are shown in the figure 2. From the figure, we can see that the first (data misfitting) term has the local minimum problem, while the second (differential semblance) term has a bigger range of convexity. After summing them together, we can solve the local minimum problem in some sense.

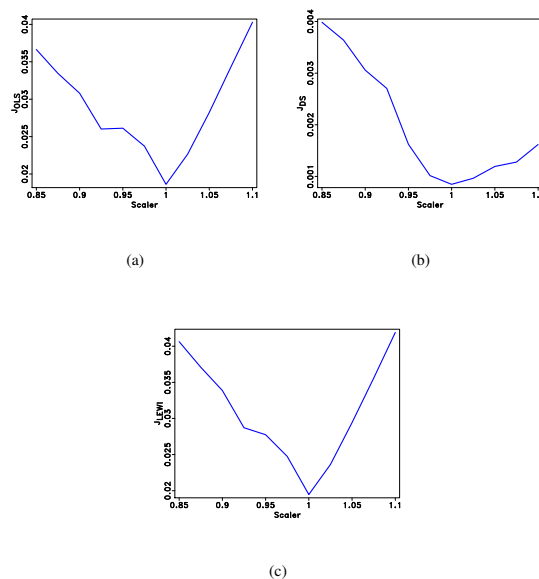


Figure 2: Scanning test of the two-term objective function (a) The first term; (b) The second term; (c) The total one.

Inversion tests on simple layer model

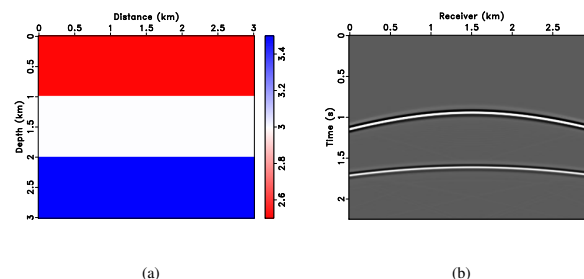


Figure 3: (a) True velocity model; (b) Synthetic shot gather at position 1.5 km.

In this section, we apply our proposed extended reflection waveform inversion in building a simple three-layer model as shown

ERWI

in figure 3(a). We use the same acquisition configuration as the last section to model synthetic data. One common shot gather at position $x_s = 1.5\text{km}$ are shown in figure 3(b).

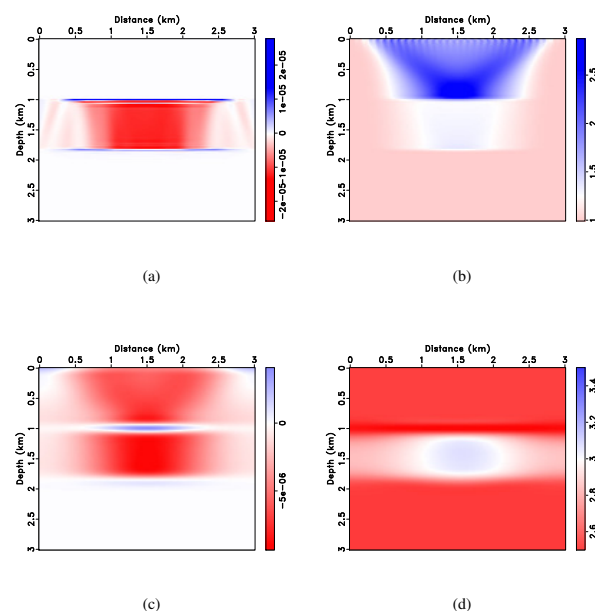


Figure 4: (a) Gradient of background velocity; (b) Diagonal of tomographic Hessian; (c) Gradient of background velocity after scaling by diagonal Hessian; (d) Inverted velocity by ERWI after 5 iterations

Then we apply ERWI to update the background velocity. The initial background velocity is constant ($v = 2.5\text{km/s}$). The gradient of background velocity, as shown in Figure 4(a), mainly provides the correct velocity update information. Figure 4(b) shows the approximation of diagonal Hessian for ERWI, which has a physical meaning of subsurface illumination. Figure 4(c) shows the scaled gradient by the diagonal Hessian, which is more balanced than 4(a). It will help accelerate the convergent rate of ERWI. Figure 4(d) shows the inverted background velocity model after 5 iterations, we can see that it almost recover the low-wavenumber components of the true model.

Using true, initial and inverted background velocity, we apply linearized inversion to obtain the inverted extended reflectivity, as shown in figure 5. All of them run 10 iterations. From the figures, we can see that, with inverted background velocity, the second layer is almost positioned at the correct depth ($z = 2\text{km}$) and most of the reflections are focused at zero offset.

CONCLUSION AND DISCUSSION

In this abstract, we introduce model extension and differential semblance optimization into reflection-based waveform inversion and show that the objective function of ERWI is convex in a larger range than difference-based waveform inversion. Two different gradients for high- and low-wavenumber components have been derived in this abstract. We also approximated the

diagonal Hessian of objective function with respect to background model and it shows information about the subsurface illumination. Numerical tests show that our proposed ERWI can successfully provide both high- and low-wavenumber components of subsurface model.

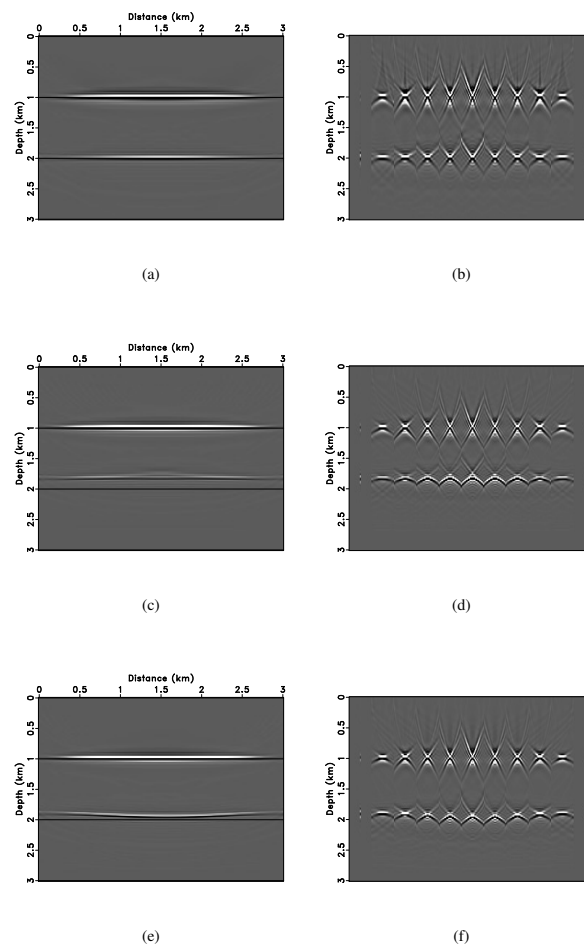


Figure 5: Extended reflectivity after linearized inversion. (a)-(b) Zero-offset image and subsurface offset image gather with correct velocity; (c)-(d): Zero-offset image and subsurface offset image gather with incorrect velocity; (e)-(f): Zero-offset image and subsurface offset image gather with inverted velocity;

However, there are still lots of work need future investigations. The most important one is improving the efficiency of ERWI. Another theoretical challenge is relaxing the linear approximation. Low frequency control (Sun and Symes, 2012) and nested inversion scheme (Almomin and Biondi, 2013) are two possible solutions.

ACKNOWLEDGMENTS

Thank the sponsors of Rice Inversion Project (TRIP) and Seismic Wave Propagation and Imaging (SWPI) for their support.

<http://dx.doi.org/10.1190/segam2014-1149.1>

EDITED REFERENCES

Note: This reference list is a copy-edited version of the reference list submitted by the author. Reference lists for the 2014 SEG Technical Program Expanded Abstracts have been copy edited so that references provided with the online metadata for each paper will achieve a high degree of linking to cited sources that appear on the Web.

REFERENCES

- Almomin, A., and B. Biondi, 2013, Tomographic full-waveform inversion (tfwi) by successive linearizations and scale separations: 83rd Annual International Meeting, SEG, Expanded Abstracts, doi: 10.1190/segam2013-1378.1.
- Biondi, B., and P. Sava, 1999, Wave-equation migration velocity analysis: 69th Annual International Meeting, SEG, Expanded Abstracts, 1723–1726.
- Biondi, B., and W. W. Symes, 2004, Angle-domain common-image gathers for migration velocity analysis by wavefield-continuation imaging: *Geophysics*, **69**, 1283–1298, <http://dx.doi.org/10.1190/1.1801945>.
- Bunks, C., F. M. Saleck, S. Zaleski, and G. Chavent, 1995, Multiscale seismic waveform inversion: *Geophysics*, **60**, 1457–1473, <http://dx.doi.org/10.1190/1.1443880>.
- Fomel, S., 2007, Shaping regularization in geophysical-estimation problems: *Geophysics*, **72**, no. 2, R29–R36, <http://dx.doi.org/10.1190/1.2433716>.
- Liu, Y., W. W. Symes, Y. Huang, and Z. Li, 2013a, Linearized extended waveform inversion via differential semblance optimization in the depth-oriented extension: Presented at the 83rd Annual International Meeting, SEG.
- Liu, Y., W. W. Symes, and Z. Li, 2013b, Multisource least-squares extended reverse-time migration with preconditioning guided gradient method: 83rd Annual International Meeting, SEG, Expanded Abstracts, doi: 10.1190/segam2013-1251.1.
- Luo, Y., and G. T. Schuster, 1991, Wave-equation travelttime inversion: *Geophysics*, **56**, 645–653, <http://dx.doi.org/10.1190/1.1443081>.
- Ma, Y., and D. Hale, 2013, Wave-equation reflection travelttime inversion with dynamic warping and hybrid waveform inversion: 83rd Annual International Meeting, SEG, Expanded Abstracts, doi: 10.1190/segam2013-0087.1.
- Rickett, J. E., and P. C. Sava, 2002, Offset and angle-domain common image-point gathers for shot-profile migration: *Geophysics*, **67**, 883–889, <http://dx.doi.org/10.1190/1.1484531>.
- Shen, P., and W. Symes, 2013, Subsurface domain image warping by horizontal contraction and its application to wave-equation migration velocity analysis: Presented at the 83rd Annual International Meeting, SEG.
- Shen, P., and W. W. Symes, 2008, Automatic velocity analysis via shot profile migration: *Geophysics*, **73**, no. 5, VE49–VE59, <http://dx.doi.org/10.1190/1.2972021>.
- Shin, C., and Y. H. Cha, 2008, Waveform inversion in the Laplace domain: *Geophysical Journal International*, **173**, no. 3, 922–931, <http://dx.doi.org/10.1111/j.1365-246X.2008.03768.x>.
- Sun, D., and W. W. Symes, 2012, Waveform inversion via nonlinear differential semblance optimization: Presented at the 82nd Annual International Meeting, SEG.

- Symes, W. W., 2008, Migration velocity analysis and waveform inversion: *Geophysical Prospecting*, **56**, no. 6, 765–790, <http://dx.doi.org/10.1111/j.1365-2478.2008.00698.x>.
- Tarantola, A., 1984, Inversion of seismic reflection data in the acoustic approximation: *Geophysics*, **49**, 1259–1266, <http://dx.doi.org/10.1190/1.1441754>.
- Van Leeuwen, T., and W. Mulder, 2010, A correlation-based misfit criterion for wave-equation traveltime tomography: *Geophysical Journal International*, **182**, no. 3, 1383–1394, <http://dx.doi.org/10.1111/j.1365-246X.2010.04681.x>.
- Virieux, J., and S. Operto, 2009, An overview of full-waveform inversion in exploration geophysics: *Geophysics*, **74**, no. 6, WCC1–WCC26, <http://dx.doi.org/10.1190/1.3238367>.
- Xu, S., D. Wang, and F. Chen, G. Lambare and Y. Zhang, 2012, Inversion on reflected seismic wave: Presented at the 82nd Annual International Meeting, SEG.
- Zhou, H., L. Amundsen, and G. Zhang, 2012, Fundamental issues in full-waveform inversion: 82nd Annual International Meeting, SEG, Expanded Abstracts, doi: 10.1190/segam2012-0878.1.